Elastic Structure Preserving Impedance Control for Nonlinearly Coupled Tendon-Driven Systems

Pollayil, George Jose*; Meng, Xuming*; Keppler, Manuel; Pfanne, Martin; Bicchi, Antonio; Ott, Christian

Elastic Structure Preserving Impedance Control for Nonlinearly Coupled Tendon-Driven Systems

George Jose Pollayil*, *Graduate Student Member, IEEE*, Xuming Meng*, Manuel Keppler, Martin Pfanne, Antonio Bicchi, *Fellow, IEEE*, and Christian Ott, *Senior Member, IEEE*

***Abstract*— Traditionally, most of the nonlinear control techniques for elastic robotic systems focused on achieving a desired closed-loop behavior by modifying heavily the intrinsic properties of the plant. This is also the case of elastic tendon-driven systems, where the highly nonlinear couplings lead to several control challenges. Following the current philosophy of exploiting the mechanical compliance rather than fighting it, this letter proposes an Elastic Structure Preserving impedance (ESPi) control for systems with coupled elastic tendinous transmissions. Our strategy achieves a globally asymptotically stable closed-loop system that minimally shapes the intrinsic inertial and elastic structure. It further allows to impose a desired link-side impedance behavior. Simulations performed on the tendon-driven index finger of the DLR robot David show satisfactory results of link-side interaction behavior and set-point regulation.**

***Index Terms*— Robotics, control applications**

I. Introduction

TAKING inspiration from nature, recent research displayed a focus on elastic and compliant design of robots. Such a trend allowed to reach high levels of energy efficiency and natural motions [1], [2]. Mechanical compliance has greatly contributed to increase the robustness of robots while interacting with the environment. For instance, the role of such a property is crucial in robotic manipulation; it allows to achieve robust grasps [3] while also aiding in coping with the impacts and interactions of the robot with the surroundings during grasp acquisition or tactile exploration. Trying to imitate how humans modulate hand compliance by controlling tendons, several articulated tendon-driven elastic robotic hands have been designed. The UB Hand III [4], the DLR David Hand [5] (Fig. 1a), the Pisa/IIT SoftHand [6], and the CEA dexterous hand [7] are some notable examples. Besides, cable-driven mechanisms are employed also in the field of robotic manipulators, e.g., [8]–[10]. On the one hand, tendon-driven systems are lightweight and compact, and feature high responsiveness. On the other hand, the control of such mechanisms present unique challenges due to the elastic couplings between joints caused by the routing and the nonlinear features of tendon elasticity.

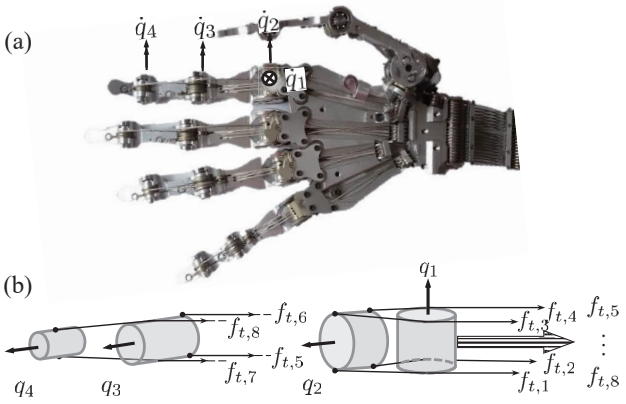

Fig. 1. An example of a tendon-driven system: (a) DLR David Hand. The joint coordinates $\boldsymbol{q} \in \mathbb{R}^4$ for the index finger are shown. (b) The routing of the index finger with coupled tendons. The directions of the tendon forces $\boldsymbol{f_t} \in \mathbb{R}^8$ are shown.

Typically, two control loops are used for achieving desired joint motions and stiffness, i.e., an inner one for realizing tendon force control and an outer one for imposing a desired link behavior. A statically decoupling method for realizing joint motion and stiffness variation was provided in [11]. Following the two-loop strategy, the authors in [12] proposed a cascaded approach with careful consideration of tendon tension constraints by solving an optimization problem. A similar method was shown in [13], where a force control law with an optimized tendon tension distribution algorithm is derived. The guarantee of stability is not provided in the aforementioned works. In a single-DoF case, [14] showed the Lyapunov stability of the impedance control with tendon-driven elastic mechanisms and adjustable linear springs. A decentralized control for motion tracking was designed for the CEA dexterous hand using a single step H_∞ optimization framework in [7]. An integrator backstepping design was employed in [15] for antagonistically actuated joints to derive an asymptotically stable control after performing an inertial decoupling using partial feedback linearization. Some other works focused also on the control of special types of tendon-driven mechanisms: e.g. PD control design is studied for

* These two authors contributed equally to this work.

George Jose Pollayil (*Corresponding Author*) and Antonio Bicchi are with the Research Center "E. Piaggio" and Dipartimento di Ingegneria dell'Informazione, Università di Pisa, Italy, and also with Soft Robotics for Human Cooperation and Rehabilitation, Istituto Italiano di Tecnologia, 16163 Genova, Italy. (e-mail: georgejose.pollayil@phd.unipi.it; antonio.bicchi@unipi.it)

Xuming Meng, Manuel Keppler, Martin Pfanne, and Christian Ott are with the Institute of Robotics and Mechatronics Center (RMC), German Aerospace Center (DLR), Müncher Str. 20, 82234 Wessling, Germany (e-mail: xuming.meng@dlr.de; manuel.keppler@dlr.de; martin.pfanne@dlr.de; christian.ott@dlr.de)

underactuated tendon-driven mechanisms in [16] and transmissions with branching tendons in [17]. Notwithstanding the effectiveness of the above works, all consist in canceling out or modifying, by means of control, the intrinsic properties with which the system is designed.

The problem of robustly controlling robots through a passive design and minimal shaping of the dynamic structure was discussed in [18]–[20]. In particular, a perfect gravity cancellation in order to allow the control of the robot without accounting for the gravity bias was studied in [19]. Instead, [20] and [21] proposed control laws for implementing a desired interaction behavior, on motor or link side respectively, while preserving the elastic structure. The concept of Elastic Structure Preserving (ESP) control was extended to bidirectional antagonistic actuation in [22], [23]. Even though [20]- [23] address the case of multi-DoF robots, the reduced elastic model employed therein cannot be used to model tendon-driven systems: thus, the ESP control cannot be applied straightforwardly to our case.

The contributions of the present letter are the following:

- we extend the ESP framework to multi-DoF tendon-driven systems with nonlinear mechanical couplings;
- we show that for such systems it is possible to achieve a desired closed-loop dynamics with an added impedance behavior on the link side while minimally modifying the dynamics and the elastic coupling;
- our control law achieves regulation of the link position to a desired value.

The validation is carried out in simulation on an elastically coupled multi-DoF finger.

II. Problem Definition

In this section, we consider the following model [24], [25], which can be applied to a wide variety of tendon-driven mechanisms, e.g. [4], [5], [8], [9] and [10].

$$\begin{cases} \boldsymbol{M}(\boldsymbol{q})\ddot{\boldsymbol{q}} + \boldsymbol{C}(\boldsymbol{q},\dot{\boldsymbol{q}})\dot{\boldsymbol{q}} + \boldsymbol{g}(\boldsymbol{q}) = \boldsymbol{\psi}(\boldsymbol{q},\boldsymbol{\theta}) + \boldsymbol{\psi}_{ext} & \text{(1a)} \\ \boldsymbol{B}\ddot{\boldsymbol{\theta}} + \boldsymbol{\tau}(\boldsymbol{q},\boldsymbol{\theta}) = \boldsymbol{u}\,, & \text{(1b)} \end{cases}$$

where, $\boldsymbol{q} \in \mathbb{R}^{n_q}$ are the joint variables, $\boldsymbol{\theta} \in \mathbb{R}^{n_\theta}$ are the motor positions, $\boldsymbol{\psi}_{ext} \in \mathbb{R}^{n_q}$ are the external link-side torques, and $\boldsymbol{u} \in \mathbb{R}^{n_\theta}$ are the control inputs. Here, n_q and n_θ are the degrees of freedom (DoF) and the degrees of actuation (DoA), respectively. Moreover, $\boldsymbol{M}$ is the link inertia, $\boldsymbol{C}$ the matrix with Coriolis and centrifugal terms. By using the Christoffel symbols, we have that $\dot{\boldsymbol{M}}(\boldsymbol{q}) - 2\boldsymbol{C}(\boldsymbol{q},\dot{\boldsymbol{q}})$ is skew-symmetric. The vector $\boldsymbol{g}$ denotes gravity torques, and $\boldsymbol{B}$ is the reflected motor inertia matrix. In most tendon-driven mechanisms, each tendon is pulled by one motor; in this work, we consider such a case.

The nonlinear coupling between link-side (1a) and motor-side dynamics (1b) is given by $\boldsymbol{\psi}(\boldsymbol{q},\boldsymbol{\theta})$ and $\boldsymbol{\tau}(\boldsymbol{q},\boldsymbol{\theta})$, which are the link-side and the motor-side elastic torques, respectively. They depend on the tendon forces $\boldsymbol{f}_t$ as follows

$$\boldsymbol{\psi}(\boldsymbol{q},\boldsymbol{\theta}) = \boldsymbol{P}^T\boldsymbol{f}_t(\boldsymbol{q},\boldsymbol{\theta}) \quad (2)$$

$$\boldsymbol{\tau}(\boldsymbol{q},\boldsymbol{\theta}) = \boldsymbol{E}\boldsymbol{f}_t(\boldsymbol{q},\boldsymbol{\theta}), \quad (3)$$

where $\boldsymbol{P} \in \mathbb{R}^{n_\theta \times n_q}$ is the so called *coupling matrix*. The matrix $\boldsymbol{E} \in \mathbb{R}^{n_\theta \times n_\theta}$ is constant and diagonal, contains the values of the motor radii, and thus it is invertible. The force profiles $\boldsymbol{f}_t$ are typically highly nonlinear functions of the tendon elongations $\Delta\boldsymbol{l}$. Moreover, (1a)-(1b) models a tendon-driven system if $\boldsymbol{f}_t > \boldsymbol{0}$. This means that the tendons are taut. Let $U_{e,j}(\Delta l_j) : \mathbb{R} \to \mathbb{R}^+$ be the elastic potential function associated with the j^{th} tendon[1], where $j = 1, \cdots, n_\theta$. Then, the corresponding tendon force is given by $f_{t,j}(\Delta l_j) := \frac{\partial U_{e,j}(\Delta l_j)}{\partial \Delta l_j}$ and satisfies the following assumption.

Assumption 1. *The tendon elongations are of the form $\Delta\boldsymbol{l} = \boldsymbol{E}\boldsymbol{\theta} - \boldsymbol{P}\boldsymbol{q}$. Moreover, the tendon force $f_{t,j}(\Delta l_j), \forall j$ is C^3 and strictly monotonously increasing w.r.t. Δl_j. Therefore, the elastic potential function $U_{e,j}(\Delta l_j)$ is convex and radially unbounded. Using the virtual work principle,*

$$\delta U_e(\Delta\boldsymbol{l}) = \delta U_e(\boldsymbol{q},\boldsymbol{\theta}) = \delta\boldsymbol{\theta}^T \underbrace{(\boldsymbol{E}\boldsymbol{f}_t)}_{:=\boldsymbol{\tau}} + \delta\boldsymbol{q}^T \underbrace{(-\boldsymbol{P}^T\boldsymbol{f}_t)}_{:=-\boldsymbol{\psi}}\,. \quad (4)$$

Assumption 2. *The coupling matrix $\boldsymbol{P}$ is constant, with $n_\theta > n_q$ and has full rank, i.e., rank$(\boldsymbol{P}) = n_q$.*

Physical Motivation of the Assumptions: The expression of the tendon elongation (cf. Sec. 6.4.2 in [25]) and the three times continuous differentiability in Assumption 1 are common to many tendon-driven systems: for instance, [4] and [5]. Additionally, the monotonous increase of $\boldsymbol{f}_t$ w.r.t. $\Delta\boldsymbol{l}$ is a standard property. Instead, the constant $\boldsymbol{P}$ in Assumption 2 can be realized with extra turns on the pulleys. Moreover, a well-designed tendon network exhibits a *coupling matrix* with full rank[2] [25].

A schematic illustration of an example of (1a)-(1b) is shown in Fig. 2a. Given the model (1a)-(1b), we have the following control objectives:

(i) achieve a desired stiffness $\boldsymbol{K}_q$ and damping $\boldsymbol{D}_q$ behavior on the link side;
(ii) achieve link regulation to a desired value $\boldsymbol{q}_d$, which means that $\boldsymbol{q} \to \boldsymbol{q}_d$ for $t \to \infty$;
(iii) minimally modify the dynamic properties, the original coupling, and the elastic structure of the system.

III. Desired Closed-loop System

To accomplish the goals stated in Sec. II, we aim to realize the desired closed-loop dynamics

$$\begin{cases} \boldsymbol{M}(\boldsymbol{q})\ddot{\boldsymbol{q}} + \boldsymbol{C}(\boldsymbol{q},\dot{\boldsymbol{q}})\dot{\boldsymbol{q}} = \boldsymbol{P}^T\boldsymbol{f}_t(\boldsymbol{q},\boldsymbol{\eta}) \\ \qquad\qquad - \boldsymbol{K}_q(\boldsymbol{q} - \boldsymbol{q}_d) - \boldsymbol{D}_q\dot{\boldsymbol{q}} + \boldsymbol{\psi}_{ext} & \text{(5a)} \\ \boldsymbol{B}\ddot{\boldsymbol{\eta}} + \boldsymbol{E}\boldsymbol{f}_t(\boldsymbol{q},\boldsymbol{\eta}) = -\boldsymbol{D}_\eta\dot{\boldsymbol{\eta}} + \boldsymbol{\tau}_p, & \text{(5b)} \end{cases}$$

which is depicted in Fig. 2b. The matrices $\boldsymbol{K}_q$, $\boldsymbol{D}_q$ and $\boldsymbol{D}_\eta$ are symmetric, positive definite and bounded. Note that here

[1] In the following, subscript j is used for numbering tendons or motors, and subscript i is used for joints.

[2] The condition on the dimensions of $\boldsymbol{P}$ is related to Caratheodory's theorem [25], which states that at least $n_q + 1$ tendons are needed to actuate a tendon-driven robot. In DLR David Hand, $n_\theta = 2n_q$ tendons are used for the thumb, index and middle fingers; $n_\theta < 2n_q$ tendons for the ring and little fingers. The routing of the index finger is shown in Fig. 1b.

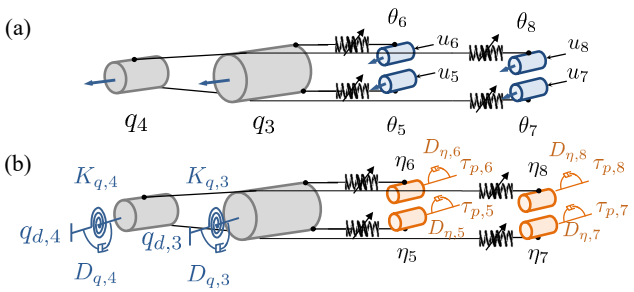

Fig. 2. (a): original system dynamics of the last two links in the index finger of DLR David Hand (Fig. 1a). (b): closed-loop dynamics achieved by implementing the proposed controller.

we introduced new virtual motor variables $\boldsymbol{\eta}$ to realize the desired link-side behavior. This coordinate transformation will be introduced in Sec. IV-A. Moreover, $\boldsymbol{\tau}_p = \boldsymbol{E}\boldsymbol{f}_{t_p}$ is a feed-forward motor torque term, where $\boldsymbol{f}_{t_p} \in \mathbb{R}^{n_\theta}$ are the desired tendon tensions, which should be chosen properly to avoid the slack of the tendons.

In (5a)-(5b) the inertial properties and elastic couplings are preserved and only the gravity term is canceled. Thus, the desired interaction behavior is obtained by minimally modifying the structure of the original system (1a)-(1b).

By defining the state vector $\boldsymbol{z} = [\boldsymbol{q}^T \ \dot{\boldsymbol{q}}^T \ \boldsymbol{\eta}^T \ \dot{\boldsymbol{\eta}}^T]^T$ and imposing $\dot{\boldsymbol{z}} = \boldsymbol{0}$ and $\boldsymbol{\psi}_{ext} = \boldsymbol{0}$ on (5a)-(5b) we get

$$\begin{cases} \boldsymbol{0} = \boldsymbol{P}^T \boldsymbol{f}_t(\boldsymbol{q}, \boldsymbol{\eta}) - \boldsymbol{K}_q(\boldsymbol{q} - \boldsymbol{q}_d) \\ \boldsymbol{E}\boldsymbol{f}_t(\boldsymbol{q}, \boldsymbol{\eta}) = \boldsymbol{\tau}_p. \end{cases} \tag{6}$$

If we choose $\boldsymbol{f}_{t_p}$ inside the nullspace $\mathcal{N}(\boldsymbol{P}^T)$ of $\boldsymbol{P}^T$, i.e. $\boldsymbol{P}^T \boldsymbol{f}_{t_p} = \boldsymbol{P}^T \boldsymbol{E}^{-1} \boldsymbol{\tau}_p = \boldsymbol{0}$, the unique equilibrium of (5a)-(5b) is

$$\boldsymbol{z}_{eq} = [\boldsymbol{q}_d^T \ \boldsymbol{0}^T \ \boldsymbol{\eta}_d^T \ \boldsymbol{0}^T]^T. \tag{7}$$

Here, $\boldsymbol{\eta}_d$ is the solution of $\boldsymbol{f}_t(\boldsymbol{q}_d, \boldsymbol{\eta}_d) = \boldsymbol{f}_{t_p}$. If (7) is asymptotically stable, we achieve the control objective (ii).

IV. Control Design

In this section, we present the control design that allows to achieve the desired dynamics (5a)-(5b). We first perform a coordinate transformation of the motor variables from $\boldsymbol{\theta}$ to $\boldsymbol{\eta}$ to achieve the desired link-side behavior and subsequently design the control law to realize the desired motor-side dynamics and stabilize the system.

A. Coordinate Transformation

To achieve the desired link-side behavior, we impose the equivalence of the n_q equations (1a) and (5a)

$$\underbrace{\boldsymbol{P}^T \boldsymbol{f}_t(\boldsymbol{q}, \boldsymbol{\theta})}_{\boldsymbol{\psi}(\boldsymbol{q},\boldsymbol{\theta})} = \underbrace{\boldsymbol{P}^T \boldsymbol{f}_t(\boldsymbol{q}, \boldsymbol{\eta})}_{\boldsymbol{\psi}(\boldsymbol{q},\boldsymbol{\eta})} + \underbrace{\boldsymbol{g}(\boldsymbol{q}) - \boldsymbol{K}_q(\boldsymbol{q} - \boldsymbol{q}_d) - \boldsymbol{D}_q \dot{\boldsymbol{q}}}_{\boldsymbol{n}(\boldsymbol{q},\dot{\boldsymbol{q}},\boldsymbol{q}_d)}. \tag{8}$$

Note that (8) represents n_q coordinate relations. As $n_\theta > n_q$, (8) does not determine a unique coordinate transformation (CT) and we have to introduce another $n_\theta - n_q$ relations

$$\underbrace{\boldsymbol{N}^T \boldsymbol{f}_t(\boldsymbol{q}, \boldsymbol{\eta})}_{\boldsymbol{\psi}_N(\boldsymbol{q},\boldsymbol{\eta})} = \underbrace{\boldsymbol{N}^T \boldsymbol{f}_t(\boldsymbol{q}, \boldsymbol{\theta})}_{\boldsymbol{\psi}_N(\boldsymbol{q},\boldsymbol{\theta})}, \tag{9}$$

where $\boldsymbol{N} \in \mathbb{R}^{n_\theta \times (n_\theta - n_q)}$ is a basis of $\mathcal{N}(\boldsymbol{P}^T)$. Equation (9) represents $n_\theta - n_q$ independent relations thanks to Assumption 2. Hence, putting together (8) and (9), we get a system of n_θ nonlinear equations

$$\underbrace{\begin{aligned} \boldsymbol{\psi}(\boldsymbol{q}, \boldsymbol{\eta}) - \boldsymbol{\psi}(\boldsymbol{q}, \boldsymbol{\theta}) + \boldsymbol{n}(\boldsymbol{q}, \dot{\boldsymbol{q}}, \boldsymbol{q}_d) = \boldsymbol{0} \\ \boldsymbol{\psi}_N(\boldsymbol{q}, \boldsymbol{\eta}) - \boldsymbol{\psi}_N(\boldsymbol{q}, \boldsymbol{\theta}) = \boldsymbol{0}. \end{aligned}}_{\boldsymbol{F}(\boldsymbol{q},\dot{\boldsymbol{q}},\boldsymbol{q}_d,\boldsymbol{\theta},\boldsymbol{\eta})=\boldsymbol{0}} \tag{10}$$

Proposition 1. *The system* (10) *represents a unique coordinate transformation from* $(\boldsymbol{q}, \boldsymbol{\theta})$ *to* $(\boldsymbol{q}, \boldsymbol{\eta})$.

Proof. We make use of the Implicit Function Theorem. Let $(\boldsymbol{q}_0, \dot{\boldsymbol{q}}_0, \boldsymbol{\theta}_0, \boldsymbol{\eta}_0)$[3] be a generic solution to (10) and let

(a) $\boldsymbol{F}$ be at least C^1,
(b) $\det(\frac{\partial \boldsymbol{F}}{\partial \boldsymbol{\eta}}) \neq 0$ and $\det(\frac{\partial \boldsymbol{F}}{\partial \boldsymbol{\theta}}) \neq 0$,

in the solution point. Then, in a neighborhood of the solution, $\forall(\boldsymbol{q}, \dot{\boldsymbol{q}}, \boldsymbol{\theta})$ there exists a unique $\boldsymbol{\eta}$ such that $\boldsymbol{F} = \boldsymbol{0}$, and $\forall(\boldsymbol{q}, \dot{\boldsymbol{q}}, \boldsymbol{\eta})$ there exists a unique $\boldsymbol{\theta}$ such that $\boldsymbol{F} = \boldsymbol{0}$. This means that, if conditions (a) and (b) are met for all admissible $(\boldsymbol{q}, \dot{\boldsymbol{q}}, \boldsymbol{\theta}, \boldsymbol{\eta})$, (10) is a unique CT from $\boldsymbol{\theta}$ to $\boldsymbol{\eta}$ globally.

Condition (a) requires that $\boldsymbol{\psi}$, $\boldsymbol{\psi}_N$ and $\boldsymbol{n}$ are C^1 functions. Assuming $\boldsymbol{q}$ and $\dot{\boldsymbol{q}}$ continuous, verifying the continuity of $\boldsymbol{n}$ is trivial, and $\boldsymbol{\psi}$ and $\boldsymbol{\psi}_N$ are C^1 thanks to Assumption 1.

As $\frac{\partial \boldsymbol{F}}{\partial \boldsymbol{\theta}} = -\frac{\partial \boldsymbol{F}}{\partial \boldsymbol{\eta}}|_{\boldsymbol{\eta}=\boldsymbol{\theta}}$, to verify condition (b) we can limit to check if $\det(\frac{\partial \boldsymbol{F}}{\partial \boldsymbol{\eta}}) \neq 0$. Using (2), (9), (10) and the property of the determinant of a product, condition (b) becomes

$$\det\left(\frac{\partial \boldsymbol{F}}{\partial \boldsymbol{\eta}}\right) = \det\left(\begin{bmatrix} \boldsymbol{P}^T \\ \boldsymbol{N}^T \end{bmatrix}\right) \det\left(\frac{\partial \boldsymbol{f}_t(\boldsymbol{q}, \boldsymbol{\eta})}{\partial \boldsymbol{\eta}}\right) \neq 0 \ . \tag{11}$$

The first determinant is always non-zero by virtue of Assumption 2 and due to the row space of $\boldsymbol{P}^T$ being orthogonal to $\mathcal{N}(\boldsymbol{P}^T)$. The second one is also non-zero thanks to Assumption 1. Thus, also condition (b) is always fulfilled. □

To find the relations between $\dot{\boldsymbol{\theta}}, \ddot{\boldsymbol{\theta}}$ and $\dot{\boldsymbol{\eta}}, \ddot{\boldsymbol{\eta}}$, differentiate (10) with respect to time to get

$$\dot{\boldsymbol{\theta}} = \boldsymbol{A}(\boldsymbol{q}, \boldsymbol{\theta}, \boldsymbol{\eta})\dot{\boldsymbol{\eta}} + \boldsymbol{a}(\boldsymbol{q}, \dot{\boldsymbol{q}}, \ddot{\boldsymbol{q}}, \boldsymbol{q}_d, \boldsymbol{\theta}, \boldsymbol{\eta}) \,, \tag{12}$$

where

$$\boldsymbol{A} = \begin{bmatrix} \frac{\partial \boldsymbol{\psi}_\theta}{\partial \boldsymbol{\theta}} \\ \frac{\partial \boldsymbol{\psi}_{N\theta}}{\partial \boldsymbol{\theta}} \end{bmatrix}^{-1} \begin{bmatrix} \frac{\partial \boldsymbol{\psi}_\eta}{\partial \boldsymbol{\eta}} \\ \frac{\partial \boldsymbol{\psi}_{N\eta}}{\partial \boldsymbol{\eta}} \end{bmatrix}; \tag{13}$$

$$\boldsymbol{a} = \begin{bmatrix} \frac{\partial \boldsymbol{\psi}_\theta}{\partial \boldsymbol{\theta}} \\ \frac{\partial \boldsymbol{\psi}_{N\theta}}{\partial \boldsymbol{\theta}} \end{bmatrix}^{-1} \left(\begin{bmatrix} \frac{\partial \boldsymbol{\psi}_\eta}{\partial \boldsymbol{q}} - \frac{\partial \boldsymbol{\psi}_\theta}{\partial \boldsymbol{q}} \\ \frac{\partial \boldsymbol{\psi}_{N\eta}}{\partial \boldsymbol{q}} - \frac{\partial \boldsymbol{\psi}_{N\theta}}{\partial \boldsymbol{q}} \end{bmatrix} \dot{\boldsymbol{q}} + \begin{bmatrix} \dot{\boldsymbol{n}} \\ \boldsymbol{0} \end{bmatrix} \right). \tag{14}$$

For easing notation, we have written $\boldsymbol{\psi}_\theta = \boldsymbol{\psi}(\boldsymbol{q}, \boldsymbol{\theta})$, $\boldsymbol{\psi}_\eta = \boldsymbol{\psi}(\boldsymbol{q}, \boldsymbol{\eta})$, $\boldsymbol{\psi}_{N\theta} = \boldsymbol{\psi}_{\boldsymbol{N}}(\boldsymbol{q}, \boldsymbol{\theta})$ and $\boldsymbol{\psi}_{N\eta} = \boldsymbol{\psi}_{\boldsymbol{N}}(\boldsymbol{q}, \boldsymbol{\eta})$. The inversion in (13)-(14) is guaranteed thanks to condition (b) in the proof of Proposition 1. Differentiating (12) again, we get the original motor accelerations expressed in $\boldsymbol{\eta}$

$$\ddot{\boldsymbol{\theta}} = \boldsymbol{A}\ddot{\boldsymbol{\eta}} + \dot{\boldsymbol{A}}\dot{\boldsymbol{\eta}} + \dot{\boldsymbol{a}}. \tag{15}$$

[3] As we are in the regulation case, $\boldsymbol{q}_d$ is fixed.

B. Control Law

Applying the CT to (1a), the link-side dynamics becomes (5a). Substituting (15) into (1b), we have $\boldsymbol{BA}\ddot{\boldsymbol{\eta}} + \boldsymbol{B}\dot{\boldsymbol{A}}\dot{\boldsymbol{\eta}} + \boldsymbol{B}\dot{\boldsymbol{a}} + \boldsymbol{E}\boldsymbol{f}_t(\boldsymbol{q},\boldsymbol{\theta}) = \boldsymbol{u}$. Applying the control law

$$\begin{aligned}\boldsymbol{u} = &\boldsymbol{B}\dot{\boldsymbol{A}}\dot{\boldsymbol{\eta}} + \boldsymbol{B}\dot{\boldsymbol{a}} + \boldsymbol{E}\boldsymbol{f}_t(\boldsymbol{q},\boldsymbol{\theta}) \\ &+ \boldsymbol{B}\boldsymbol{A}\boldsymbol{B}^{-1}(-\boldsymbol{E}\boldsymbol{f}_t(\boldsymbol{q},\boldsymbol{\eta}) - \boldsymbol{D}_\eta\dot{\boldsymbol{\eta}} + \boldsymbol{\tau}_p).\end{aligned} \tag{16}$$

to cancel unwanted terms, and multiplying both sides by $\boldsymbol{B}(\boldsymbol{BA})^{-1}$, we obtain the desired dynamics (5a)-(5b). For further understanding, and for a block diagram of the ESP concept, refer [20], which treats the case of elastic robots with $n_\theta = n_q$.

V. Stability and Passivity Analyses

A. Stability Analysis

To analyze the stability properties of (7), consider the function $V = T + U_q + \bar{U}_e$, where

$$T(\boldsymbol{q},\dot{\boldsymbol{q}},\dot{\boldsymbol{\eta}}) = \frac{1}{2}\dot{\boldsymbol{q}}^T\boldsymbol{M}(\boldsymbol{q})\dot{\boldsymbol{q}} + \frac{1}{2}\dot{\boldsymbol{\eta}}^T\boldsymbol{B}\dot{\boldsymbol{\eta}}\,; \tag{17}$$

$$U_q(\boldsymbol{q}) = \frac{1}{2}(\boldsymbol{q}-\boldsymbol{q}_d)^T\boldsymbol{K}_q(\boldsymbol{q}-\boldsymbol{q}_d)\,; \tag{18}$$

$$\bar{U}_e(\boldsymbol{q},\boldsymbol{\eta}) = U_e(\boldsymbol{q},\boldsymbol{\eta}) - \underbrace{(\boldsymbol{E}\boldsymbol{\eta}-\boldsymbol{P}\boldsymbol{q})^T\boldsymbol{f}_{t_p}}_{U_p = -\Delta\boldsymbol{l}(\boldsymbol{q},\boldsymbol{\eta})^T\boldsymbol{f}_{t_p}}. \tag{19}$$

Here, T is the virtual kinetic energy and U_q and U_p are the potential energies in (5a)-(5b): U_q due to the link-side spring and U_p due to $\boldsymbol{\tau}_p = \boldsymbol{E}\boldsymbol{f}_{t_p}$. By virtue of Assumption 1 and (4) and as $\boldsymbol{f}_{t_p} \in \mathcal{N}(\boldsymbol{P}^T)$,

$$\left(\frac{\partial\bar{U}_e}{\partial\boldsymbol{q}}\right)^T = -\boldsymbol{P}^T\boldsymbol{f}_t(\boldsymbol{q},\boldsymbol{\eta}) + \cancelto{\boldsymbol{0}}{\boldsymbol{P}^T\boldsymbol{f}_{t_p}}; \tag{20}$$

$$\left(\frac{\partial\bar{U}_e}{\partial\boldsymbol{\eta}}\right)^T = \boldsymbol{E}\boldsymbol{f}_t(\boldsymbol{q},\boldsymbol{\eta}) - \boldsymbol{E}\boldsymbol{f}_{t_p}. \tag{21}$$

Proposition 2. *The equilibrium point* (7) *of the closed-loop system* (5a)-(5b) *is globally asymptotically stable (GAS) in absence of the external torques* $\boldsymbol{\psi}_{ext}$ [4].

Proof. We employ the Global Invariant Set Theorem (Theorem 3.5 in [26]). Note that V is a scalar function with continuous first partial derivatives. Moreover, as U_e is radially unbounded (Assumption 1), so is also V. Differentiating V w.r.t. time, substituting (20)-(21), $\ddot{\boldsymbol{q}}$ from (5a) and $\ddot{\boldsymbol{\eta}}$ from (5b), and due to the skew-symmetry of $\dot{\boldsymbol{M}}(\boldsymbol{q}) - 2\boldsymbol{C}(\boldsymbol{q},\dot{\boldsymbol{q}})$,

$$\begin{aligned}\dot{V} = &-\dot{\boldsymbol{q}}^T\boldsymbol{C}(\boldsymbol{q},\dot{\boldsymbol{q}})\dot{\boldsymbol{q}} + \frac{1}{2}\dot{\boldsymbol{q}}^T\dot{\boldsymbol{M}}(\boldsymbol{q})\dot{\boldsymbol{q}} \\ &- \dot{\boldsymbol{q}}^T\boldsymbol{D}_q\dot{\boldsymbol{q}} - \dot{\boldsymbol{\eta}}^T\boldsymbol{D}_\eta\dot{\boldsymbol{\eta}} + \dot{\boldsymbol{q}}^T\boldsymbol{\psi}_{ext} \\ = &-\dot{\boldsymbol{q}}^T\boldsymbol{D}_q\dot{\boldsymbol{q}} - \dot{\boldsymbol{\eta}}^T\boldsymbol{D}_\eta\dot{\boldsymbol{\eta}} + \dot{\boldsymbol{q}}^T\boldsymbol{\psi}_{ext}\,.\end{aligned} \tag{22}$$

Substituting $\boldsymbol{\psi}_{ext} = \boldsymbol{0}$ in (22) makes $\dot{V}$ negative semi-definite. Consider the set $R = \{\boldsymbol{z} \in \mathbb{R}^{2n_q+2n_\theta} | \dot{V}(\boldsymbol{z}) = 0\}$. To find the largest invariant set in R, notice that for any solution $\boldsymbol{z}(t)$ belonging to R, we have that $\dot{\boldsymbol{q}} \equiv \boldsymbol{0}$, $\dot{\boldsymbol{\eta}} \equiv \boldsymbol{0} \implies \ddot{\boldsymbol{q}} \equiv \boldsymbol{0}, \ddot{\boldsymbol{\eta}} \equiv \boldsymbol{0}$. Considering (5a) and (5b), we can conclude that $\boldsymbol{z}(t) \equiv \boldsymbol{z}_{eq}$ is the only solution that can remain in R. Knowing that the equilibrium point (7) is the largest invariant set in R concludes the proof.

□

B. Passivity Analysis

From Proposition 2, it follows that the scalar term U_p in V is bounded since $\boldsymbol{q}$, $\boldsymbol{\eta}$ and $\boldsymbol{f}_{t_p}$ are bounded. Therefore, there exists a constant $c \in \mathbb{R} : S = V + c$ is positive semi-definite. Thus, we choose S as storage function.

Proposition 3. *The closed-loop system* (5a)-(5b) *is an output-strict passive (OSP) map from the external link-side torques* $\boldsymbol{\psi}_{ext}$ *to the velocities* $\dot{\boldsymbol{q}}$.

Proof. Differentiating S w.r.t. time and following analogous steps as done for $\dot{V}$ in the proof of Proposition 2 we get

$$\dot{S} = -\dot{\boldsymbol{q}}^T\boldsymbol{D}_q\dot{\boldsymbol{q}} - \dot{\boldsymbol{\eta}}^T\boldsymbol{D}_\eta\dot{\boldsymbol{\eta}} + \dot{\boldsymbol{q}}^T\boldsymbol{\psi}_{ext}\,. \tag{23}$$

Thanks to the positive definiteness of $\boldsymbol{D}_q$, there exists $\epsilon > 0$ such that $\dot{S} \leq \dot{\boldsymbol{q}}^T\boldsymbol{\psi}_{ext} - \epsilon\dot{\boldsymbol{q}}^T\dot{\boldsymbol{q}}$.

□

VI. Validation

In this section, we perform a validation of the proposed control method in simulation using the tendon-driven index finger of the DLR David Hand [5]. As shown in Fig. 1b, the index finger has 4 DoF, and 8 DoA with nonlinear tendon coupling. The dynamic and elastic parameters in (1a)-(1b) are taken from the real robot. The simulations are performed in MATLAB & SIMULINK using a variable-step Runge-Kutta45 solver. The design of $\boldsymbol{D}_q$ and $\boldsymbol{D}_\eta$ is done by using modal damping factors $\boldsymbol{\xi}_q$ and $\boldsymbol{\xi}_\eta$ as in Eq. (85) in [20]. The derivatives of the dynamic matrices are computed using the strategies in [27]. Then, $\ddot{\boldsymbol{q}}$ and $\boldsymbol{q}^{(3)}$ are obtained through model-based calculations[5], which require an estimation of the external torques. Furthermore, (10) is solved numerically using `fmincon` interior-point algorithm. In order to include the effect of sensor noise, we add zero-mean band-limited white noise with 1kHz sampling rate to q_i and θ_j, which fits to our practical case. Thus, the noise will propagate to the velocity, acceleration and jerk as well. The noise variances at $\ddot{q}_i$ and $q_i^{(3)}$ are ca. $1\,\mathrm{rad/s^2}$ and $10^3\,\mathrm{rad/s^3}$, respectively. Two tests are carried out: one for regulation to $\boldsymbol{q}_d$ and another assessing the effective achievement of the commanded stiffness $\boldsymbol{K}_q$.

A. Regulation

The first test shows the regulation behavior. The reference joint value is changed at time $t = 1\,\mathrm{s}$ from $\boldsymbol{q}_0 = \boldsymbol{0}\,\mathrm{deg}$ (open finger) to $\boldsymbol{q}_d = [0, 40, 60, 40]^T\,\mathrm{deg}$ (semi-closed finger); see Fig. 4. At $t = 4\,\mathrm{s}$, a constant $\boldsymbol{\psi}_{ext} = [-0.4, -0.25, -0.15, -0.05]\,\mathrm{Nm}$ is applied to each link. The aim is to simulate the finger closing and an interaction with the external environment. Due to the small link inertia compared

[4] Showing the stability of the equilibrium (7) of (5a)-(5b) is sufficient to prove the stability of the corresponding one in the original coordinates. Indeed, the equilibrium in $\boldsymbol{q}$ and $\boldsymbol{\theta}$ can be obtained using (10) and (12).

[5] The link acceleration $\ddot{\boldsymbol{q}} = \boldsymbol{M}^{-1}(\boldsymbol{\psi} + \boldsymbol{\psi}_{ext} - \boldsymbol{C}\dot{\boldsymbol{q}} - \boldsymbol{g})$ and the jerk $\boldsymbol{q}^{(3)} = \boldsymbol{M}^{-1}(\dot{\boldsymbol{\psi}} + \dot{\boldsymbol{\psi}}_{ext} - \dot{\boldsymbol{M}}\ddot{\boldsymbol{q}} - \dot{\boldsymbol{C}}\dot{\boldsymbol{q}} - \boldsymbol{C}\ddot{\boldsymbol{q}} - \dot{\boldsymbol{g}})$.

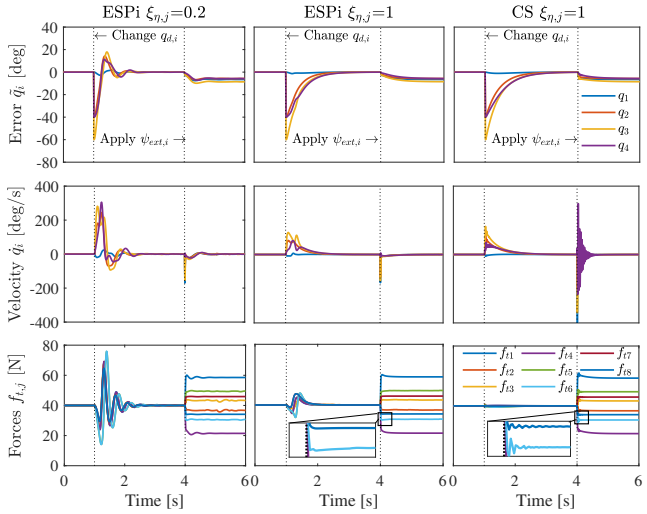

Fig. 3. The results of regulation behavior when the modal damping factors $\boldsymbol{\xi_{\eta_j} = 0.2}$ and $\boldsymbol{\xi_{\eta_j} = 1}$ for the ESPi and $\boldsymbol{\xi_{\theta_j} = 1}$ for the CS controller. The rows from top to bottom show the regulation errors $\tilde{\boldsymbol{q}} = \boldsymbol{q} - \boldsymbol{q_d}$, the joint velocities $\dot{\boldsymbol{q}}$ and the tendon forces $\boldsymbol{f_t(q, \theta)}$. At $\boldsymbol{t = 1\,s}$ and $\boldsymbol{t = 4\,s}$, $\boldsymbol{q_d}$ and $\boldsymbol{\psi_{ext}}$ are changed, respectively. Higher-frequency oscillations in tendon forces are present in CS controller (bottom plot of the third column).

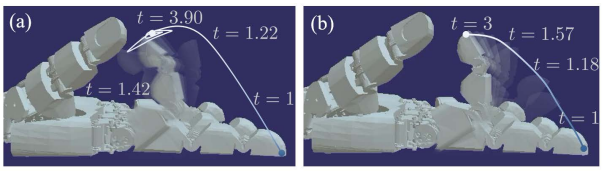

Fig. 4. Finger motions during regulation: (a) ESPi $\boldsymbol{\xi_{\eta_j} = 0.2}$ and (b) ESPi $\boldsymbol{\xi_{\eta_j} = 1}$. The timestamps correspond to the time axis in Fig. 3.

to motor inertia, changing ξ_{q_i} will have little effect on the damping. Therefore, we consider two different damping settings, where the link-side damping factor is always $\xi_{q_i} = 0.6$, while the motor-side damping is chosen as $\xi_{\eta_j} = 0.2$ or $\xi_{\eta_j} = 1$. The commanded stiffness is chosen near to the mean value of the intrinsic joint stiffness and is $\boldsymbol{K}_q = \mathrm{diag}(3.5, 2.5, 1, 0.5)\,\mathrm{Nm/rad}$. Furthermore, for all tendons, the initial and the desired pretension are $f_{t_{p,j}} = 40\,\mathrm{N}, \forall j$ (about one third of the maximum f_{t_j} for the DLR David Hand), which is inside the $\mathcal{N}(\boldsymbol{P}^T)$. We also compare our method with the controller with cascaded structure (CS) proposed in [12] as it has similar control objectives as ours. For the CS controller, we use the same $\boldsymbol{K}_q$. We implement the same modal damping design for $\boldsymbol{D}_q$ as we did in ESPi controller. The inner-loop gain $\boldsymbol{K}_\tau$ (cf. Eq.(10) in [12]) is chosen such that the regulation error $\tilde{\boldsymbol{q}} = \boldsymbol{q} - \boldsymbol{q}_d$ in $t \in [1, 4]\,\mathrm{s}$ is similar. To make the two controllers comparable, we add also a damping term on the motor side.

The results are displayed in Fig. 3. By comparing the results of ESPi controller in first and second columns, for $\xi_{\eta_j} = 1$, there is no overshoot (see first row) and the peak velocities (second row) are smaller than when $\xi_{\eta_j} = 0.2$. Moreover, $\forall j$, the actual tendon force $f_{t,j}(q_1, \cdots, q_4, \theta_j)$ fulfills $\boldsymbol{f}_t > \boldsymbol{0}$, varies less with higher damping and converges to the desired pretension $f_{t_{p,j}}$. The corresponding motions of the finger are displayed in Fig. 4; notice the absence of oscillations for

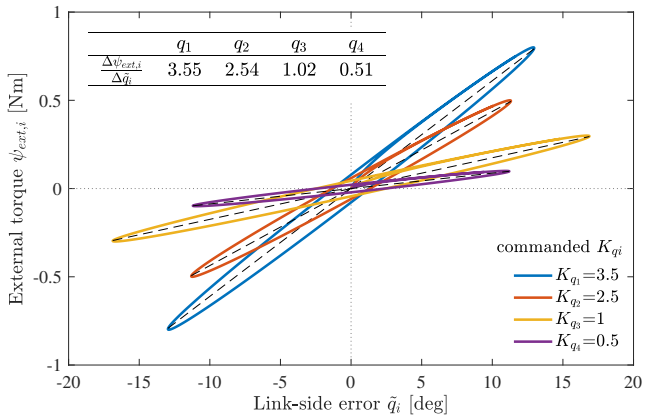

Fig. 5. External torques $\boldsymbol{\psi_{ext}}$ vs. the link-side errors $\tilde{\boldsymbol{q}} = \boldsymbol{q} - \boldsymbol{q_d}$. The colored lines represent the external torques with different commanded $\boldsymbol{K_{q_i}}$ in $\mathrm{N\,m/rad}$. The dashed black lines are the commanded stiffness values. The achieved stiffness, approximated by $\frac{\boldsymbol{\Delta\psi_{ext,i}}}{\boldsymbol{\Delta q_i}}$ is reported in the top left.

$\xi_{\eta_j} = 1$. When $t \in [1, 4]\,\mathrm{s}$, $\tilde{\boldsymbol{q}}$ converges to zero. Instead, from $t = 4\,\mathrm{s}$, Fig. 3 shows the disturbance rejection behavior. The links show the expected transient behavior and converge to the shifted equilibrium $\boldsymbol{q}^\star$ satisfying $\boldsymbol{K}_q(\boldsymbol{q}^\star - \boldsymbol{q}_d) = \boldsymbol{\psi}_{ext}$, which evaluates to $\boldsymbol{q}^\star = [-6.55, -5.73, -8.59, -5.73]\,\mathrm{deg}$. Both the ESPi (second column) and CS controllers (third column) achieve similar link-side regulation behavior. Observe that $\dot{\boldsymbol{q}}$ in CS controller has higher-frequency oscillations in the transient phase, which are mainly caused by tendon oscillations (third row), which could be rather harmful; they can drastically reduce the lifetime and lead to the damage of the tendons [28]. However, the variation of $f_{t,j}$ at $t = 1\mathrm{s}$ in ESPi controller is larger than the ones in CS. Both the controllers show satisfactory disturbance rejection and robustness to sensor noise.

B. Interaction Behavior

The second test consists in validating the achieving of the desired stiffness during interaction: while the finger is commanded to hold a desired $\boldsymbol{q}_d$, we apply sine waves as external torques $\boldsymbol{\psi}_{ext}$ and record the resulting link-side errors $\tilde{\boldsymbol{q}} = \boldsymbol{q} - \boldsymbol{q}_d$. The achieved stiffness is approximated by $\frac{\Delta\psi_{ext,i}}{\Delta\tilde{q}_i}$, i.e., the slope of a linear regression of $\psi_{ext,i}$ versus $\tilde{q}_i$. We employed the following parameters: $\xi_{q_i} = 0.6$, $\xi_{\eta_j} = 1$ and the same previous $\boldsymbol{q}_d$ and $\boldsymbol{K}_q$. The external torques $\boldsymbol{\psi}_{ext}$ had the amplitudes $[0.8, 0.5, 0.3, 0.1]^T\mathrm{Nm}$ as they are the maximum bearable joint torque values. The sine waves had a frequency of 1Hz to simulate a typical human interaction behavior. The desired pretension is the same as before.

The results are shown in Fig. 5. The achieved stiffness is near to the commanded. It can be seen from Fig. 5 that the measured data do not fully lie on the commanded stiffness (dashed black lines). This is due to $\dot{\boldsymbol{q}}$ and $\ddot{\boldsymbol{q}}$ not reaching zero during the application of $\boldsymbol{\psi}_{ext}$ except for the points with maximum amplitude. Hence, the transient dynamics is reflected in ellipse-like shapes.

VII. Conclusions

This letter extended the Elastic Structure Preserving impedance control concept, first introduced for non-redundant elastic robots in [20], [21], to tendon-driven systems featuring nonlinear elastic coupling with constant coupling matrix and with monotonously increasing tendon-force profiles. The resulting controller achieves globally asymptotically stable set-point regulation and simultaneously imposes a desired link-side impedance and tendon pretension. Moreover, the proven output-strict passivity allows also to claim $\mathcal{L}_2$ stability (Theorem 6.5 in [29]). The underlying idea evolves introducing a change of motor coordinates that encodes the desired link-side impedance behavior. Notably, the resulting closed loop preserves the inertial properties and only minimally shapes the elastic structure due to the added link-side impedance. This minimal shaping is expected to produce favorable results regarding the controller's energy efficiency and robustness. The evaluation was carried out in simulation on a tendon-driven finger with elastic couplings demonstrating a satisfactory set-point regulation behavior and robustness against external disturbances and sensor noise. The results further show that the desired link impedance is successfully implemented. In the control design and in simulation, we did not consider static or viscous friction. However, if a suitable friction model or observer is available, compensation is possible on both the link and motor sides. Without proper compensation, static friction would create a steady-state error during regulation and the viscous one would cause more damping in the transient. On a real robot, the implementation requires sensing motor positions and estimating joint positions from tendon elongations, which can be measured through magnetic sensors. A measure or estimation of the external torques is also needed. Future work would include an experimental validation of the conservation of the elastic structure and extension to the case of non-constant *coupling matrix*.

References

[1] M. G. Catalano, G. Grioli, M. Garabini, F. Bonomo, M. Mancini, N. Tsagarakis, and A. Bicchi, "VSA-Cubebot: A modular variable stiffness platform for multiple degrees of freedom robots," in *2011 IEEE International Conference on Robotics and Automation*. IEEE, 2011, pp. 5090–5095.

[2] B. Vanderborght, B. Verrelst, R. Van Ham, M. Van Damme, D. Lefeber, B. M. Y. Duran, and P. Beyl, "Exploiting natural dynamics to reduce energy consumption by controlling the compliance of soft actuators," *The International Journal of Robotics Research*, vol. 25, no. 4, pp. 343–358, 2006.

[3] B. S. Homberg, R. K. Katzschmann, M. R. Dogar, and D. Rus, "Robust proprioceptive grasping with a soft robot hand," *Autonomous Robots*, vol. 43, no. 3, pp. 681–696, 2019.

[4] F. Lotti, P. Tiezzi, G. Vassura, L. Biagiotti, G. Palli, and C. Melchiorri, "Development of UB Hand 3: Early results," in *Proceedings of the 2005 IEEE International Conference on Robotics and Automation*. IEEE, 2005, pp. 4488–4493.

[5] M. Grebenstein, M. Chalon, W. Friedl, S. Haddadin, T. Wimböck, G. Hirzinger, and R. Siegwart, "The hand of the DLR hand arm system: Designed for interaction," *The International Journal of Robotics Research*, vol. 31, no. 13, pp. 1531–1555, 2012.

[6] M. G. Catalano, G. Grioli, E. Farnioli, A. Serio, C. Piazza, and A. Bicchi, "Adaptive synergies for the design and control of the Pisa/IIT softhand," *The International Journal of Robotics Research*, vol. 33, no. 5, pp. 768–782, 2014.

[7] M. Grossard, J. Martin, and G. F. da Cruz Pacheco, "Control-oriented design and robust decentralized control of the CEA dexterous robot hand," *IEEE/ASME Transactions on Mechatronics*, vol. 20, no. 4, pp. 1809–1821, 2014.

[8] S. Ma, H. Yoshinada, and S. Hirose, "CT ARM-I: Coupled tendon-driven manipulator model i-design and basic experiments," in *Proceedings 1992 IEEE International Conference on Robotics and Automation*. IEEE Computer Society, 1992, pp. 2094–2095.

[9] B. Rooks, "The harmonious robot," *Industrial Robot: An International Journal*, 2006.

[10] T. Lens and O. von Stryk, "Design and dynamics model of a lightweight series elastic tendon-driven robot arm," in *2013 IEEE International Conference on Robotics and Automation*. IEEE, 2013, pp. 4512–4518.

[11] T. Wimbock, C. Ott, A. Albu-Schäffer, A. Kugi, and G. Hirzinger, "Impedance control for variable stiffness mechanisms with nonlinear joint coupling," in *2008 IEEE/RSJ International Conference on Intelligent Robots and Systems*. IEEE, 2008, pp. 3796–3803.

[12] M. Chalon, W. Friedl, J. Reinecke, T. Wimboeck, and A. Albu-Schäffer, "Impedance control of a non-linearly coupled tendon driven thumb," in *2011 IEEE/RSJ International Conference on Intelligent Robots and Systems*. IEEE, 2011, pp. 4215–4221.

[13] M. E. Abdallah, R. Platt Jr, and C. W. Wampler, "Decoupled torque control of tendon-driven fingers with tension management," *The International Journal of Robotics Research*, vol. 32, no. 2, pp. 247–258, 2013.

[14] R. Ozawa and H. Kobayashi, "A new impedance control concept for elastic joint robots," in *2003 IEEE International Conference on Robotics and Automation (Cat. No. 03CH37422)*, vol. 3. IEEE, 2003, pp. 3126–3131.

[15] M. Chalon and B. d'Andréa Novel, "Backstepping experimentally applied to an antagonistically driven finger with flexible tendons," *IFAC Proceedings Volumes*, vol. 47, no. 3, pp. 217–223, 2014.

[16] R. Ozawa, K. Hashirii, and H. Kobayashi, "Design and control of underactuated tendon-driven mechanisms," in *2009 IEEE International Conference on Robotics and Automation*. IEEE, 2009, pp. 1522–1527.

[17] D. Sawada and R. Ozawa, "Joint control of tendon-driven mechanisms with branching tendons," in *2012 IEEE International Conference on Robotics and Automation*. IEEE, 2012, pp. 1501–1507.

[18] C. Della Santina, M. Bianchi, G. Grioli, F. Angelini, M. Catalano, M. Garabini, and A. Bicchi, "Controlling soft robots: balancing feedback and feedforward elements," *IEEE Robotics & Automation Magazine*, vol. 24, no. 3, pp. 75–83, 2017.

[19] A. De Luca and F. Flacco, "Dynamic gravity cancellation in robots with flexible transmissions," in *49th IEEE Conference on Decision and Control (CDC)*. IEEE, 2010, pp. 288–295.

[20] M. Keppler, D. Lakatos, C. Ott, and A. Albu-Schäffer, "Elastic structure preserving (ESP) control for compliantly actuated robots," *IEEE Transactions on Robotics*, vol. 34, no. 2, pp. 317–335, 2018.

[21] M. Keppler, D. Lakatos, C. Ott, and A. Albu-Schäffer, "Elastic structure preserving impedance (ESPi) control for compliantly actuated robots," in *2018 IEEE/RSJ International Conference on Intelligent Robots and Systems (IROS)*, 2018, pp. 5861–5868.

[22] R. Mengacci, M. Keppler, M. Pfanne, A. Bicchi, and C. Ott, "Elastic structure preserving control for compliant robots driven by agonistic-antagonistic actuators (ESPaa)," *IEEE Robotics and Automation Letters*, vol. 6, no. 2, pp. 879–886, 2021.

[23] X. Meng, M. Keppler, and C. Ott, "Elastic structure preserving impedance control of bidirectional antagonistic variable stiffness actuation," in *2021 European Control Conference (ECC 2021)*, July 2021, pp. 263–269. [Online]. Available: https://elib.dlr.de/143334/

[24] M. W. Spong, "Modeling and control of elastic joint robots," *Journal of Dynamic Systems, Measurement, and Control*, vol. 109, no. 4, pp. 310–318, dec 1987.

[25] R. M. Murray, Z. Li, and S. S. Sastry, *A mathematical introduction to robotic manipulation*. CRC press, 2017.

[26] J.-J. E. Slotine, W. Li *et al.*, *Applied nonlinear control*. Prentice hall Englewood Cliffs, NJ, 1991, vol. 199, no. 1.

[27] G. Garofalo, C. Ott, and A. Albu-Schäffer, "On the closed form computation of the dynamic matrices and their differentiations," in *2013 IEEE/RSJ International Conference on Intelligent Robots and Systems*, 2013, pp. 2364–2359.

[28] M. Wehr, A. Pott, and K.-H. Wehking, "Bending fatigue strength and lifetime of fiber ropes," in *Cable-Driven Parallel Robots*, C. Gosselin, P. Cardou, T. Bruckmann, and A. Pott, Eds. Cham: Springer International Publishing, 2018, pp. 73–84.

[29] H. K. Khalil, *Nonlinear control*. Pearson Higher Ed, 2014.